












RESEARCH ARTICLE | OCTOBER 18 2023

High-performance photothermal effect in MOCVD grown topological insulator Sb_2Te_3 nanograting

Xin Li ; Zhengfen Wan ; Yinan Zhang ; Yachao Zhang ; Yanlei Hu ; Zengji Yue  ; Arun Kumar ; Raimondo Cecchini ; Massimo Longo  

 Check for updates

Appl. Phys. Lett. 123, 163104 (2023)

<https://doi.org/10.1063/5.0166420>



View Online



Export Citation

Articles You May Be Interested In

Magnetic proximity effect in the heterostructures of topological insulators and $SrRuO_3$

Appl. Phys. Lett. (May 2023)

Detection and tuning of spin-orbit interactions on inclined-grown Bi_2O_2Se nanoplates

Appl. Phys. Lett. (January 2022)

Wafer-scale MOCVD grown WS_2 with normally off transistor behavior and its general application on different amorphous substrates

Appl. Phys. Lett. (October 2023)



Applied Physics Letters

Special Topics Open for Submissions

[Learn More](#)

High-performance photothermal effect in MOCVD grown topological insulator Sb_2Te_3 nanograting

Cite as: Appl. Phys. Lett. **123**, 163104 (2023); doi: [10.1063/5.0166420](https://doi.org/10.1063/5.0166420)

Submitted: 5 July 2023 · Accepted: 25 September 2023 ·

Published Online: 18 October 2023



View Online



Export Citation



CrossMark

Xin Li,^{1,2} Zhengfen Wan,¹ Yinan Zhang,¹ Yachao Zhang,³ Yanlei Hu,³ Zengji Yue,^{1,a)} Arun Kumar,^{4,b)} Raimondo Cecchini,^{4,c)} and Massimo Longo^{4,5,a)}

AFFILIATIONS

¹Institute of Photonic Chips, University of Shanghai for Science and Technology, Shanghai 200093, China

²Centre for Artificial-Intelligence Nanophotonics, School of Optical-Electrical and Computer Engineering, University of Shanghai for Science and Technology, Shanghai 200093, China

³CAS Key Laboratory of Mechanical Behavior and Design of Materials, Key Laboratory of Precision Scientific Instrumentation of Anhui Higher Education Institutes, Department of Precision Machinery and Precision Instrumentation, University of Science and Technology of China, Hefei 230027, China

⁴CNR-IMM, Agrate Brianza, Via Olivetti, 2, 20864 Agrate Brianza, Italy

⁵Department of Chemical Science and Technologies, University of Rome Tor Vergata, Via della Ricerca Scientifica, 100133 Rome, Italy

^{a)}Authors to whom correspondence should be addressed: Zengjiyue@usst.edu.cn and Massimo.Longo@uniroma2.it

^{b)}Current address: Department of Physics, University of Salerno, Via Giovanni Paolo II, 132, 84084 Fisciano SA, Italy.

^{c)}Current address: CNR-IMM, Bologna, via P. Gobetti, 101, 40129 Bologna, Italy.

ABSTRACT

Photothermal energy has been widely used in high-tech applications, such as heating/cooling systems, bio-imaging, bio-sensing, and medical therapies. However, conventional photothermal materials have narrow photo-absorption bandwidth and low photothermal conversion efficiency. Innovative materials that can more efficiently harvest photothermal energy are highly demanded. Topological insulator materials with excellent optical properties hold great potential in photo-absorption and photothermal conversion. This work investigated and engineered photo-absorption and photothermal effect in Sb_2Te_3 topological insulator nanograting. The TI material was grown by metal-organic chemical vapor deposition to exploit the benefits of the process, yielding high material quality and large deposition areas. Through a meticulous process encompassing material synthesis, engineering, and characterization, highly absorptive Sb_2Te_3 topological insulator nanograting and efficient photothermal conversion have been achieved. This research contributes to the advancement of the fundamental knowledge of light-matter interaction and photothermal effects in topological insulator materials. The outcomes of this study can benefit the development of efficient photothermal materials for high-performance nano-energy and biomedical technologies.

© 2023 Author(s). All article content, except where otherwise noted, is licensed under a Creative Commons Attribution (CC BY) license (<http://creativecommons.org/licenses/by/4.0/>). <https://doi.org/10.1063/5.0166420>

Photoenergy can be transformed to photothermal or photoelectrical energy via efficient photo-absorbers performing photothermal effect.¹ Photothermal effect is the generation of thermal energy (heat) in the photo-absorbers that is widely used in energy technologies, such as generating photothermal electricity,² heating/cooling effects,³ water evaporation,⁴ and actuators.⁵ In addition, the photothermal effect also signifies in chemical and medical engineering applications, including photothermal detectors,⁶ imaging,⁷ therapy,⁸ and biosensing.⁹ Plasmonic nanoparticles (NPs) generating photothermal effect have been used for vaporization of water and optofluidic effects.¹⁰ When subjected to light irradiation, microfluidic channels facilitate the

precise manipulation to transport biomolecules and living cells at controlled speeds and directions. In nanomedicine, plasmonic NPs have the potential for designing novel optically active reagents for simultaneous molecular imaging and photothermal cancer therapy.^{11,12} The photothermal effect has also been used for selectively ablating tissues with localized heating and triggers the release payload molecules of therapeutic importance.¹²

Metallic NPs, such as Au and Ag, and dielectric NPs, such as Si and Ge, are typically used as conventional photothermal nanomaterials, in which surface plasmons and Mie resonances play a key role in photo-absorption and photothermal conversion. In addition, some

complex nanocomposites, such as AuAl₂:AlN nanoparticles,¹³ SiO₂/Au nanoshells, and SiO₂/Au/Fe₃O₄ nanoshells,¹⁴ have also been utilized for photothermal conversion. Recently, tellurium (Te) has been discovered to be a high-performance photothermal material, showcasing remarkable characteristics based on analogous principles.¹⁵ In metallic materials, surface plasmon resonance (SPR) leads to strong field enhancement and photo-absorption in the presence of electromagnetic radiation.^{16,17} The metallic NPs experience robust carrier oscillations induced by the intense electromagnetic field, giving photothermal effects. The absorption of thermal energy leads to an increase in temperature in the vicinity of the NPs. Photothermal effects are especially strong in the frequency regime of SPRs, depending on the parameters including shape, size, and organization of the NPs. High refractive index dielectrics, such as Si and Ge, can achieve nanoscale light localization based on Mie resonances and have the advantage of less optical losses.^{18,19} Similar to SPRs, Mie resonances can also enhance optical absorption when the incident photon energy is larger than the bandgap.²⁰ The dielectric NPs have been used in optical heating, coloration, and enhancing the efficiency of photovoltaic devices.^{21,22}

The assessment of an absorber system's performance is important to its operational efficiency, based on the bandwidth and light absorption efficiency. The conventional photo-absorbers have a drawback of narrow operational bandwidths. This leads to a high demand of new materials with broad-band light absorption, which generates high-performance photothermal effects. Topological insulators (TIs) represent a class of topological materials characterized by a dielectric-like bulk state coexisting with a metallic surface state.^{23–25} The metallic surface state of TIs is protected by symmetry principles, specifically particle number conservation and time reversal symmetry. A series of well-known thermoelectric semiconductors, such as Bi₂Se₃, Bi₂Te₃, and Sb₂Te₃, have been identified as TIs.^{26,27} They exhibit a range of distinctive electronic properties, such as spin-momentum locking of Dirac electrons leading to potential applications in next generation spintronic and quantum computing.^{28,29} TIs possess a multitude of unique and superior properties, making them highly versatile and applicable in various high-performance optoelectronic devices.^{30–33} Recently, Bi₂Se₃ nanostructures have been used for photothermal energy conversion^{34,35} and photothermal therapy at near infrared.³⁶ Bi₂Se₃ nanosheets displayed efficient photo-absorption and highly efficient photothermal within specific waveband. The results suggested that the nanoscale TIs could provide an excellent means to achieve highly efficient photothermal conversion in biomedical applications.

TIs demonstrate dielectric-like optical properties within the infrared frequency range, characterized by photon energies that are smaller than the bulk bandgap. Their refractive indices and extinction coefficients are much higher than those of Ge and Si in the infrared range. The dielectric-like nature of the bulk states in TI-NPs facilitates the occurrence of robust Mie resonances and efficient photo-absorption. Therefore, TIs have the very unusual property of displaying SPRs at ultraviolet, visible, far infrared to THz ranges while demonstrating Mie resonances primarily in the infrared frequency range.³⁷ They are anticipated to have efficient photo-absorption and photothermal conversion capabilities across the solar spectrum. This study showcases the manipulation of efficient photo-absorption and photothermal effects in TI nanogratings through the implementation of geometrical designs, nanofabrication techniques, comprehensive characterization,

simulations, and photothermal measurements. The experiments were performed on Sb₂Te₃ layers deposited by metal organic chemical vapor deposition (MOCVD), an advanced deposition technique featured by a high process control, large area deposition, and industrial transferability.³⁸ In particular, previous reports have demonstrated the TI insulator character of the Sb₂Te₃ films employed in the current study.^{39,40} Efficient photo-absorption and photothermal effects have been observed for harvesting energy, photothermal biosensing, and nanotherapy. This advancement promises broad applicability in photothermal nanosurgery, photochemistry, nanofabrication, and photothermal signal modulation, driving progress across these fields.

A nanograting structure was meticulously designed to achieve broad-spectrum photothermal effects. The Sb₂Te₃ thin films were synthesized using the MOCVD technique on a SiO₂ substrate. Prior to the deposition process, the substrates underwent a pre-annealing step inside the MOCVD reactor chamber at a temperature of 500 °C. This pre-annealing step aimed to eliminate the adsorbates present on the substrates, namely, physisorbed and chemisorbed water. Furthermore, the Sb₂Te₃ thin films were deposited at room temperature, by flowing the SbCl₃ and bis(trimethylsilyl)telluride [Te(SiMe₃)₂, DSMTe] precursors, with partial pressures of 2.23×10^{-4} and 3.25×10^{-4} mbar, respectively. Post-annealing treatment of the films after the growth was carried out inside the reactor at 300 °C. Comprehensive information about the growth procedure and the physical-chemical characterization of the Sb₂Te₃ thin films can be found in Refs. 38 and 41. In particular, in Ref. 38, we have reported that the root mean square roughness of a 32.4 nm-thick Sb₂Te₃ layer deposited on SiO₂, obtained by x-ray reflectivity, is 4.5 nm; therefore, for the 50 nm thick Sb₂Te₃ layers grown under the same conditions in this work, we estimate a roughness in the range of 5–10 nm. Moreover, the structural analysis of Ref. 38 has evidenced that the Sb₂Te₃ layers on SiO₂ exhibit a partial alignment of the Sb₂Te₃ grains, resulting in highly textured films oriented along the out-of-plane [001] direction.

Figure 1 shows the principle wherein SPRs enhance the photo-absorption and photothermal effects in Sb₂Te₃ nanomaterials, which are classified as TIs. The photothermal effect process can be schematically presented as (1) the incident light irradiates onto the nanograting, where the structural characteristics of the grating facilitate its coupling with electromagnetic fields. This coupling leads to the activation of SPR on the Sb₂Te₃ nanograting. Simultaneously, an incident light portion passing through the grating is reflected by the gold mirror, further intensifying the photo-absorption effect. Given the remarkable photo-absorption exhibited by TIs, this study endeavors to enhanced efficient photothermal effects through the design of a nanograting structure. The primary objective is to achieve efficient photothermal conversion and broad-spectrum photothermal absorption. (2) The occurrence of the SPR effect at the grating surface, in conjunction with the SPR on the gold mirror, results in an amplified absorption of photon energy. (3) Consequently, energy transfer from the incident light to the electrons within the Sb₂Te₃ nanograting occurs, leading to carrier oscillations and generation of a non-equilibrium carrier density. (4) During the transition toward equilibrium, inter-band carrier-carrier scatters known as Coulomb thermalization takes place. This process involves the transfer of absorbed energy to the lattice, resulting in an increase in temperature within the Sb₂Te₃ material. (5) The transferred energy manifests as heat, which is subsequently dissipated to the surrounding medium, causing an overall temperature elevation.

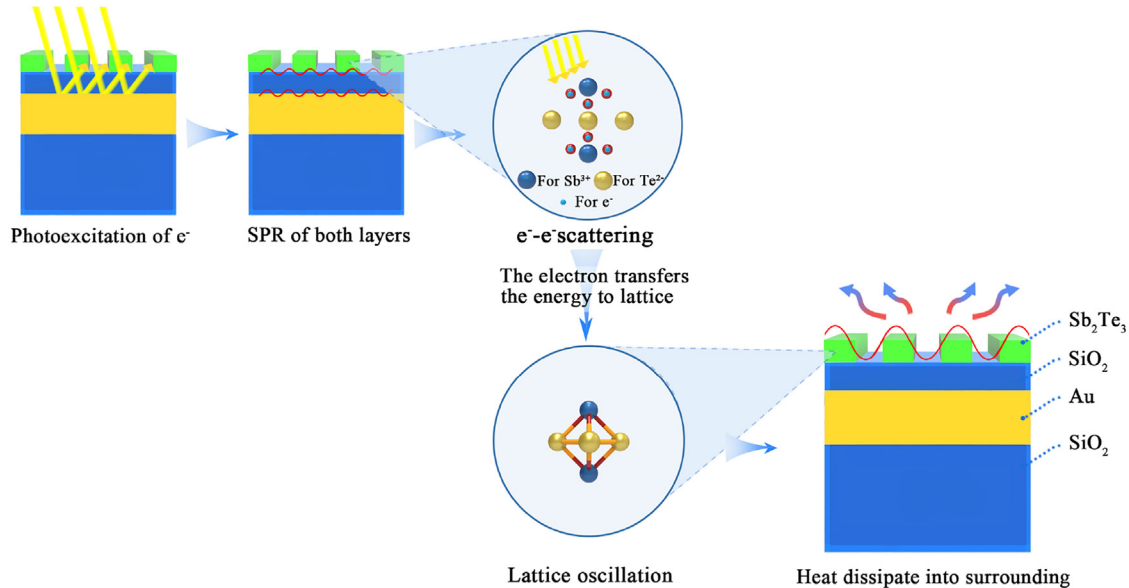


FIG. 1. Schematic diagram of interaction in the device when irradiated by light. The energy will be transferred to heat by the oscillation of lattice, which is activated by lattice absorbed light energy.

TI Sb_2Te_3 nanogratings have been fabricated by the focused ion beam lithography (FIB) method. The morphology of designed nanostructures has been characterized using scanning electron microscopy (SEM). The influence of plasmon resonances in TI nanograting was simulated using Lumerical FDTD solutions. Various light sources with different wavelengths were chosen for the simulations to investigate the effect of these resonances. The Sb_2Te_3 nanograting, with its specific structural configuration as depicted in Fig. 2(a), demonstrates several advantages. This enhancement surpasses the capabilities of previous designs in 3D structured graphene, in which the temperature reaches 80°C .⁴² The Sb_2Te_3 nanograting enables a higher density of hybridized localized SPR, thereby promoting effective light absorption over a wide range of wavelengths. Moreover, the grating structure of Sb_2Te_3 nanograting enables the coupling of incident light into the air gap, thereby enhancing the photo-absorption effect even further. The specific

structural configuration of the Sb_2Te_3 nanograting, as depicted in Fig. 2(a), involves a thickness (d), width (w), and period (p) of 50, 150, and 300 nm, respectively. Within the structure, a SiO_2 spacer layer, with a thickness (d_s) of 50 nm, is interposed. The gold mirror, with a thickness of 150 nm, serves a dual purpose. First, it reflects the incident light back toward the TI nanograting, and then, it also actively engages in SPR coupling with the SPR within the TI nanograting, enhancing the overall optical performance. This sophisticated arrangement significantly enhances the absorption characteristics of the TIs while preventing destructive interference between the incident light and the reflected light from the bottom.

The absorption [Fig. 2(b)] and reflection [Fig. 2(c)] properties of the Sb_2Te_3 nanograting are meticulously simulated using the finite-difference time-domain (FDTD) method. Remarkably, the TI device with 150 nm width exhibits an absorption rate surpassing 85% across

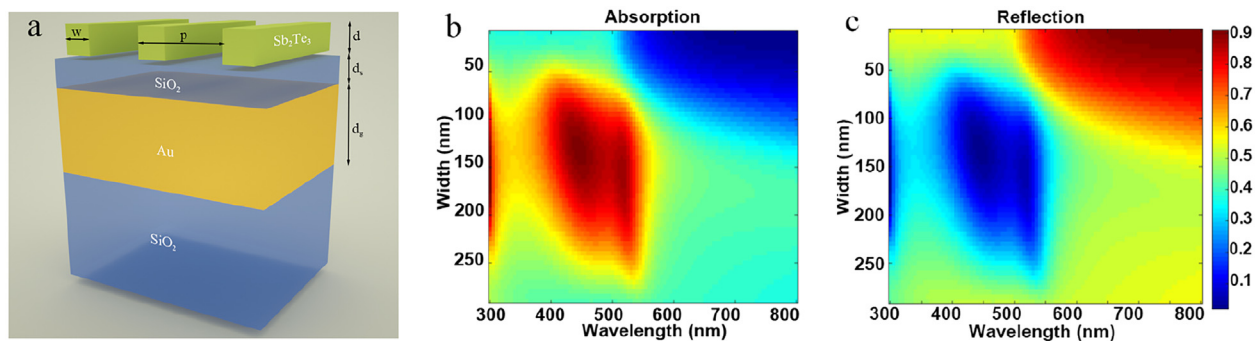


FIG. 2. (a) Schematic structure of the TI nanograting. The green bars on top form the Sb_2Te_3 TI nanograting; then, the second layer is a SiO_2 spacer and a gold mirror forms the third layer. Here, w , p , and d indicate the width, period, and thickness of the grating, respectively. It also shows " d_s " and " d_g " for the thickness of the spacer layer and gold mirror, respectively; (b) absorption vs wavelength and width of nanograting; (c) reflection vs wavelength and the width of nanograting.

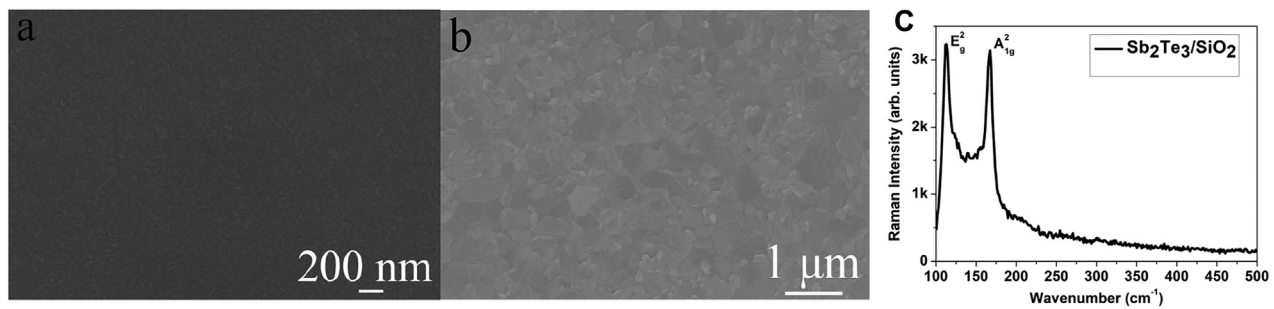


FIG. 3. (a) and (b) Scanning electron microscopy (SEM) micrographs of the TI film; (c) Raman spectrum of the TI film at the wavelength of 532 nm laser beam.

the entire 350–550 nm wavelength range. This range encompasses the near-ultraviolet to mid-visible spectrum. The extensive coverage achieved by the Sb₂Te₃ nanograting underscores its significant potential in facilitating efficient light absorption across a wide range of wavelengths.

Figures 3(a) and 3(b) provide visual evidence of the high-quality TI film obtained through the MOCVD. The images demonstrate exceptional continuity across a relatively extensive surface area while maintaining excellent flatness at the micrometer scale. The Raman spectrum analysis [Fig. 3(c)] conducted at room temperature using a Raman system, showcases two dominant peaks at about 112 and 167 cm⁻¹, which correspond to the E_g²(TO), and A_{1g}²(LO) modes of Sb₂Te₃, respectively.⁴³ A detailed investigation on the Sb₂Te₃ growth and physico-chemical characterization is reported elsewhere.^{38,41}

The photothermal performance of the TI nanograting was characterized by a high-resolution IR thermometer. The temperature increase resulting from the photothermal effects was observed and measured using both thermometers and thermocouples. Figure 4(a) shows the top-view scanning electron microscopy (SEM) image of the fabricated TI Sb₂Te₃ nanograting, where the white bar with a length of 3 μm serves as a scale reference, highlighting the distinct grating structure. Additionally, Fig. 4(b) shows the cross-sectional profile of the nanograting, with a discernible gap of ~150 nm. This dimension aligns perfectly with the optimal absorption structure identified in prior simulations. Thus, the topological insulator Sb₂Te₃ nanograting has been meticulously fabricated and designed to mirror the specifications established in our simulation models.

We have studied the photothermal effects and the influence of light polarization on the light absorption and photothermal effects in the Sb₂Te₃ nanograting. In the process of rotating the polarizer, the

photothermal images in the Sb₂Te₃ nanograting demonstrate periodic variations, as illustrated in Fig. 5. The sample is illuminated under a 450 nm blue laser. The result suggests a relation between light polarization and light absorption of nanograting. This relationship demonstrated an important role of polarization in modulating the plasmon resonances and light absorption. When the polarization is optimally oriented, there is a notable enhancement in absorption and photothermal effects. These lead to an elevation in the sample temperature, reaching peaks above 100 °C and averaging around 60 °C. This could be attributed to the interaction of polarized light and Sb₂Te₃ surface plasmons. The results clearly show the dependence of photothermal effects on light polarization.

The incorporation of TI materials facilitates efficient light-matter interactions, enabling the device to capture a substantial amount of incident light within the targeted spectral range. TIs demonstrate efficient photo-absorption over the broad-band spectrum as they have both plasmonic and dielectric-like properties. TI nanograting enable localized SPRs to effectively absorb light, which provides impedance matching for efficient reflection reduction and coupling to the optical modes. Therefore, the nanograting structure enables high photo-absorption throughout wide spectrum regimes and acts as the efficient light absorber. In real TIs, the surface conductance is frequently accompanied by non-insulating bulk conductance, resulting from bulk defects in the material.⁴⁴ Typically, the Fermi energy in TI materials resides within either the conduction band or the valence band, rather than within the expected bulk bandgap.⁴⁵ The presence of intrinsic defects induces the generation of carriers, which in turn gives rise to SPRs and high photo-absorption within the ultraviolet (UV) to visible frequency range. Most TIs, such as Sb₂Te₃, have very high extinction coefficients in the UV to infrared frequency range. The high

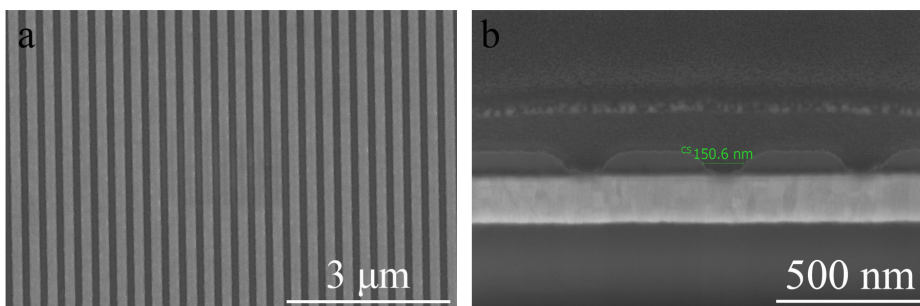


FIG. 4. (a) Top SEM image of a fabricated TI Sb₂Te₃ nanograting; (b) SEM profile image of the nanograting.

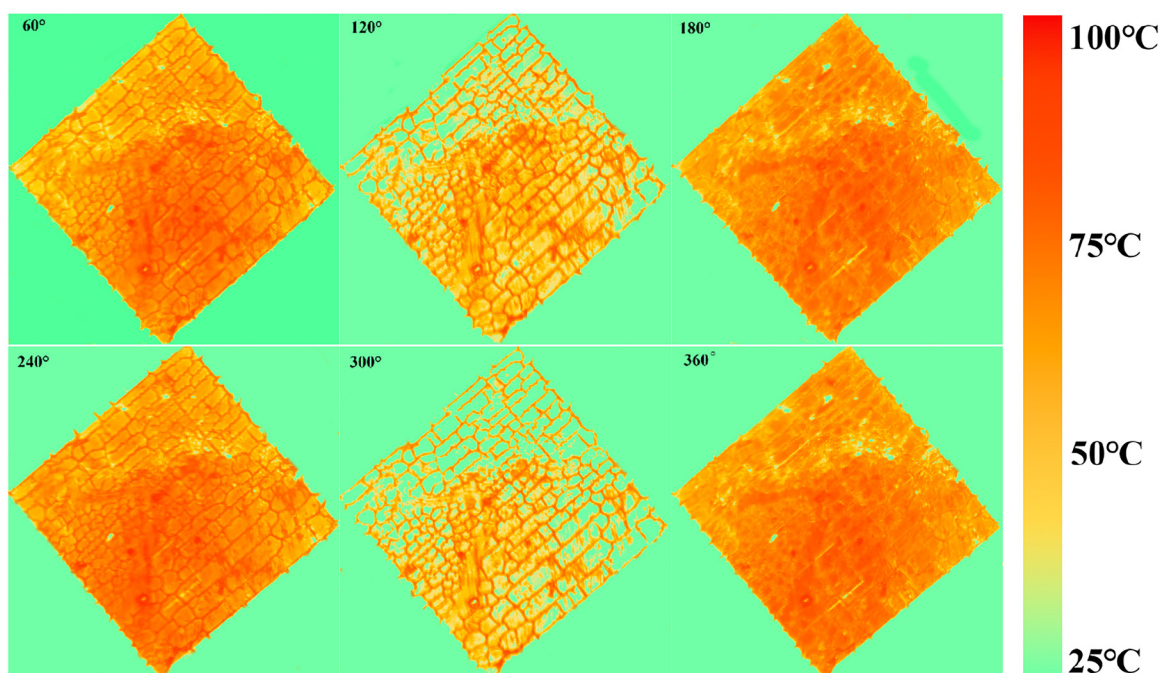


FIG. 5. Light polarization angle-dependent photothermal images in TI Sb_2Te_3 nanograting under 450 nm laser illumination.

absorption efficiency observed in the Sb_2Te_3 nanograting cannot be solely attributed to the remarkable properties of TI materials, but rather stems from the meticulous engineering and optimization of the grating structure. This emphasizes the critical role of deliberate design choices and structural configurations in achieving efficient light absorption in TI-based systems. By precisely designing the dimensions and periodicity of the grating, we have achieved the desired resonance conditions, ensuring maximum light absorption.

This work presents the development of a nanograting device composed of a TI material, which demonstrates high-performance in terms of absorption efficiency of up to 85% within the 300~500 nm spectrum. In steady-state conditions, the device reaches temperatures exceeding 100 °C, with an average temperature surpassing 60 °C. This is a significant advance in comparison of the Bi_2Se_3 film and Bi_2Se_3 nanoflower.³⁵ The TI nanogratings are demonstrated to possess outstanding photothermal conversion capabilities owing to high photo-absorption in broad spectrum. The photothermal performance shows to be improved with advantages in TI materials compared with noble metals and dielectric materials. This research expands the practical applications of TI materials in photonic energy devices, and TI-based photothermal heating will hold promise for non-contact temperature control of heating on the nanoscale.

In conclusion, we developed TI nanograting for the high-performance photothermal effect and photothermal energy conversion. The designed TI nanograting with 300 nm period and 50 nm depth demonstrates high photo-absorption in 300–500 nm wavelength ranges. The high photo-absorption leads to strong photothermal effect, and the temperature increases remarkably in the nanograting area. This work proves that TI materials are suitable for photo-absorption devices and photothermal conversion devices. The exploration of the

photothermal effect in TI nanogratings has the potential to promote the development of solar thermal energy technologies and increases the utilization of solar energy resources. This development can find wide applications in various fields including photothermal nanosurgery, photochemistry, nanofabrication, and photothermal signal modulation. This work could serve as a valuable reference for advanced investigations in energy harvesting, sensor development, quantum computing, and optoelectronic devices using topological insulators, thereby providing a springboard for innovative solutions in these fields.

We acknowledge the valuable discussion and assistance in simulation from Dr. Haoran Ren, Dr. Han Lin, and Gengde Lin. This research was supported by the Shanghai Municipal Science and Technology Major Project, Science and Technology Commission of Shanghai Municipality (No. 21DZ1100500), Shanghai Frontiers Science Center Program 2021–2025 (No. 20), and Major Scientific and Technological Projects in Anhui Province (No. 202203a05020014).

AUTHOR DECLARATIONS

Conflict of Interest

The authors have no conflicts to disclose.

Author Contributions

Xin Li: Formal analysis (equal); Investigation (equal); Methodology (equal); Writing – original draft (equal); Writing – review & editing (equal). **Zhengfen Wan:** Formal analysis (equal); Writing – original

draft (equal). **Yinan Zhang**: Formal analysis (equal); Investigation (equal). **Yachao Zhang**: Investigation (equal); Methodology (equal). **Yanlei Hu**: Investigation (equal); Methodology (equal). **Zengji Yue**: Conceptualization (equal); Formal analysis (equal); Investigation (equal); Supervision (equal); Validation (equal); Writing – original draft (equal); Writing – review & editing (equal). **Arun Kumar**: Formal analysis (equal); Investigation (equal); Methodology (equal). **Raimondo Cecchini**: Investigation (equal); Methodology (equal). **Massimo Longo**: Investigation (equal); Methodology (equal); Writing – review & editing (equal).

DATA AVAILABILITY

The data that support the findings of this study are available from the corresponding authors upon reasonable request.

REFERENCES

- ¹Y. Tian and C.-Y. Zhao, *Appl. Energy* **104**, 538–553 (2013).
- ²E. Miyako, C. Hosokawa, M. Kojima, M. Yudasaka, R. Funahashi, I. Oishi, Y. Hagihara, M. Shichiri, M. Takashima, K. Nishio, and Y. Yoshida, *Angew. Chem., Int. Ed.* **50**(51), 12266–12270 (2011).
- ³M. J. Crane, X. Zhou, E. J. Davis, and P. J. Pauzauskie, *Chem. - Asian J.* **13**(18), 2575–2586 (2018).
- ⁴G. Liu, J. Xu, and K. Wang, *Nano Energy* **41**, 269–284 (2017).
- ⁵T. Wang, D. Torres, F. E. Fernández, C. Wang, and N. Sepúlveda, *Sci. Adv.* **3**(4), e1602697 (2017).
- ⁶M. Tokeshi, M. Uchida, A. Hibara, T. Sawada, and T. Kitamori, *Anal. Chem.* **73**(9), 2112–2116 (2001).
- ⁷D. Boyer, P. Tamarat, A. Maali, B. Lounis, and M. Orrit, *Science* **297**(5584), 1160–1163 (2002).
- ⁸L. R. Hirsch, R. J. Stafford, J. A. Bankson, S. R. Sershen, B. Rivera, R. E. Price, J. D. Hazle, N. J. Halas, and J. L. West, *Proc. Natl. Acad. Sci. U. S. A.* **100**(23), 13549–13554 (2003).
- ⁹P. Zijlstra, P. M. R. Paulo, and M. Orrit, *Nat. Nanotechnol.* **7**, 379 (2012).
- ¹⁰G. L. Liu, J. Kim, Y. Lu, and L. P. Lee, *Nat. Mater.* **5**, 27 (2006).
- ¹¹X. Huang, I. H. El-Sayed, W. Qian, and M. A. El-Sayed, *J. Am. Chem. Soc.* **128**(6), 2115–2120 (2006).
- ¹²D. Pissuwan, S. M. Valenzuela, and M. B. Cortie, *Trends Biotechnol.* **24**(2), 62–67 (2006).
- ¹³M. Bilokur, A. Gentle, M. D. Arnold, M. B. Cortie, and G. B. Smith, *Sol. RRL* **1**(10), 1700092 (2017).
- ¹⁴R. Bardhan, W. Chen, M. Bartels, C. Perez-Torres, M. F. Botero, R. W. McAninch, A. Contreras, R. Schiff, R. G. Pautler, N. J. Halas, and A. Joshi, *Nano Lett.* **10**(12), 4920–4928 (2010).
- ¹⁵C. Ma, J. Yan, Y. Huang, C. Wang, and G. Yang, *Sci. Adv.* **4**(8), eaas9894 (2018).
- ¹⁶K. Aydin, V. E. Ferry, R. M. Briggs, and H. A. Atwater, *Nat. Commun.* **2**, 517 (2011).
- ¹⁷N. Liu, M. Mesch, T. Weiss, M. Hentschel, and H. Giessen, *Nano Lett.* **10**(7), 2342–2348 (2010).
- ¹⁸R. M. Bakker, D. Permyakov, Y. F. Yu, D. Markovich, R. Paniagua-Domínguez, L. Gonzaga, A. Samusev, Y. Kivshar, B. Luk'yanchuk, and A. I. Kuznetsov, *Nano Lett.* **15**(3), 2137–2142 (2015).
- ¹⁹I. Sinev, I. Iorsh, A. Bogdanov, D. Permyakov, F. Komissarenko, I. Mukhin, A. Samusev, V. Valuckas, A. I. Kuznetsov, B. S. Luk'yanchuk, A. E. Miroshnichenko, and Y. S. Kivshar, *Laser Photonics Rev.* **10**(5), 799–806 (2016).
- ²⁰L. Cao, J.-S. Park, P. Fan, B. Clemens, and M. L. Brongersma, *Nano Lett.* **10**(4), 1229–1233 (2010).
- ²¹G. P. Zograf, M. I. Petrov, D. A. Zuev, P. A. Dmitriev, V. A. Milichko, S. V. Makarov, and P. A. Belov, *Nano Lett.* **17**(5), 2945–2952 (2017).
- ²²P. Matheu, S. H. Lim, D. Derkacs, C. McPheeters, and E. T. Yu, *Appl. Phys. Lett.* **93**(11), 113108 (2008).
- ²³M. Z. Hasan and C. L. Kane, *Rev. Mod. Phys.* **82**(4), 3045–3067 (2010).
- ²⁴X.-L. Qi and S.-C. Zhang, *Rev. Mod. Phys.* **83**(4), 1057–1110 (2011).
- ²⁵A. Kumar, R. Cecchini, L. Locatelli, C. Wiemer, C. Martella, L. Nasi, L. Lazzarini, R. Mantovan, and M. Longo, *Cryst. Growth Des.* **21**(7), 4023–4029 (2021).
- ²⁶Y. Ando, *J. Phys. Soc. Jpn.* **82**(10), 102001 (2013).
- ²⁷A. Bake, Q. Zhang, C. S. Ho, G. L. Causer, W. Zhao, Z. Yue, A. Nguyen, G. Akhgar, J. Karel, D. Mitchell, Z. Pastuovic, R. Lewis, J. H. Cole, M. Nancarrow, N. Valanoor, X. Wang, and D. Cortie, *Nat. Commun.* **14**(1), 1693 (2023).
- ²⁸B. A. Bernevig, T. L. Hughes, and S.-C. Zhang, *Science* **314**(5806), 1757–1761 (2006).
- ²⁹X.-L. Wang, S. X. Dou, and C. Zhang, *npj Asia Mater.* **2**, 31–38 (2010).
- ³⁰Z. Yue, B. Cai, L. Wang, X. Wang, and M. Gu, *Sci. Adv.* **2**(3), e1501536 (2016).
- ³¹Z. Yue, G. Xue, J. Liu, Y. Wang, and M. Gu, *Nat. Commun.* **8**, 15354 (2017).
- ³²Z. Yue, H. Ren, S. Wei, J. Lin, and M. Gu, *Nat. Commun.* **9**(1), 4413 (2018).
- ³³J. Yuan, W. Ma, L. Zhang, Y. Lu, M. Zhao, H. Guo, J. Zhao, W. Yu, Y. Zhang, K. Zhang, H. Y. Hoh, X. Li, K. P. Loh, S. Li, C.-W. Qiu, and Q. Bao, *ACS Photonics* **4**(12), 3055–3062 (2017).
- ³⁴J. Guozhi, W. Peng, Z. Yanbang, and C. Kai, *Sci. Rep.* **6**, 25884 (2016).
- ³⁵Y. Liu, Y. Zhang, Z. Zhao, and G. Jia, *AIP Adv.* **8**(5), 055013 (2018).
- ³⁶H. Xie, Z. Li, Z. Sun, J. Shao, X.-F. Yu, Z. Guo, J. Wang, Q. Xiao, H. Wang, Q.-Q. Wang, H. Zhang, and P. K. Chu, *Small* **12**(30), 4136–4145 (2016).
- ³⁷H. Lu, Z. Yue, Y. Li, Y. Zhang, M. Zhang, W. Zeng, X. Gan, D. Mao, F. Xiao, T. Mei, W. Zhao, X. Wang, M. Gu, and J. Zhao, *Light. Sci. Appl.* **9**(1), 191 (2020).
- ³⁸M. Rimoldi, R. Cecchini, C. Wiemer, A. Lamperti, E. Longo, L. Nasi, L. Lazzarini, R. Mantovan, and M. Longo, *RSC Adv.* **10**(34), 19936–19942 (2020).
- ³⁹E. Longo, M. Belli, M. Alia, M. Rimoldi, R. Cecchini, M. Longo, C. Wiemer, L. Locatelli, P. Tsipas, A. Dimoulas, G. Gubbiotti, M. Fanciulli, and R. Mantovan, *Adv. Funct. Mater.* **32**(4), 2109361 (2022).
- ⁴⁰R. Cecchini, R. Mantovan, C. Wiemer, L. Nasi, L. Lazzarini, and M. Longo, *Phys. Status Solidi* **12**(8), 1800155 (2018).
- ⁴¹M. Rimoldi, R. Cecchini, C. Wiemer, E. Longo, S. Cecchi, R. Mantovan, and M. Longo, *Cryst. Growth Des.* **21**(9), 5135–5144 (2021).
- ⁴²K.-T. Lin, H. Lin, T. Yang, and B. Jia, *Nat. Commun.* **11**(1), 1389 (2020).
- ⁴³G. C. Sossio, S. Caravati, and M. Bernasconi, *J. Phys.* **21**(9), 095410 (2009).
- ⁴⁴D. Kong, Y. Chen, J. J. Cha, Q. Zhang, J. G. Analytis, K. Lai, Z. Liu, S. S. Hong, K. J. Koski, S.-K. Mo, Z. Hussain, I. R. Fisher, Z.-X. Shen, and Y. Cui, *Nat. Nanotechnol.* **6**(11), 705–709 (2011).
- ⁴⁵J. Zhang, C.-Z. Chang, Z. Zhang, J. Wen, X. Feng, K. Li, M. Liu, K. He, L. Wang, X. Chen, Q.-K. Xue, X. Ma, and Y. Wang, *Nat. Commun.* **2**, 574 (2011).